Journal of Current Veterinary Research

ISSN: 2636-4026

Journal homepage: http://www.jcvr.journals.ekb.eg

Anatomy

Intra Ocular and Orbital Dimension of the Dog Eye (Canis familiaris)

Rania Taher[1]*, Mohamed Abdo[2] and Atef Erasha[1]

(1) Department of Anatomy and Embryology, Faculty of Veterinary Medicine, University of Sadat City, Sadat City 32897, Egypt.

(2) Department of Anatomy and Embryology, Faculty of Veterinary Medicine, Badr University Cairo, Badr City 11829, Egypt.

**Corresponding author:* vet_haitham@yahoo.com *Received: 24/12/2021 Accepted: 11/1/2022*

ABSTRACT

Intraocular diseases, for instance, cataract, and blindness due to the globe diseases require precise measurement of ophthalmic parameters as these diseases may affect the treatment and management of cases. Additionally, understanding species intraocular parameters using computed tomography (CT) scanning is crucial for appropriate diagnosis. There is little literature concerning about intraocular and orbital parameters of domestic dogs. Therefore, this study aimed to describe the computed tomography features of the dog eye and its intraocular parameters dimension. Animal heads that not suffering from any diseases related to the eye were disarticulated, then a CT scan was performed. The radiodensity of the lens, anterior chamber, vitreous chamber, where density for right and left eye were (13.92, 14.49), (10.25, 11.60), (129.16, 129.64) respectively. Also, various orbital dimensions were measured. The present study's findings represent a first step toward developing CT reference values for domestic dog intraocular structural assessments.

Keywords: Computed tomography; Goat; Intraocular structures; Orbit

INTRODUCTION

Eye protection when considering lens replacement surgery to treat cataracts, blindness due to the globe disease, and radiotherapy as a sort of interventional therapy, require determining the measurements of the intraocular parameters. Also, the knowledge of the CT features of the dog eye can serve to increase the diagnostic, therapeutic, and preventive management of ocular diseases, whether they are kept for human rescued, or used in research (Lantyer-Araujo et al., 2019). Ocular MRI and Ultrasound are the modalities of choice in cases of ophthalmological disease (Penninck et al., 2001), (Kumawat & Jhirwal, 2021). In contrast, CT is more effective at analyzing the orbital cortical bone than MRI and takes less time to scan (Morgan et al., 1994), (Dennis, 2000).

CT provides imaging of orbital soft tissues and ocular adnexa with high spatial and moderate contrast resolution. Multiplanar diagnostic imaging has improved the diagnosis of ocular diseases in human beings and animals. Nowadays, good-quality images and 3D reconstructions achieve better identification and resolution of extra and intraocular structures than previously.

Many publications related to US and MRI of canine ocular structures had been published (Penninck et al., 2001), (Boroffka et al., 2008),(Vosough et al., 2009), (Singh et al., 2015), (Vinas et al., 2019), (Kovaļčuka & Mūrniece, 2020), (Kumawat & Jhirwal, 2021),

(Yilmaz & Durmaz, 2021), but few CT researches that describe the intraocular parameters and normal appearance within normal eyes (Salgüero et al., 2015), (El-naseery et al., 2016), (Chiwitt et al., 2017), (Lantyer-Araujo et al., 2019), (Chandrakumar et al., 2019). Thus this study aimed to describe the normal CT appearance of domestic dog eye, orbital parameters, described and measured dimensions, and radiodensities of intraocular structures using CT scan within presumed normal dog eye.

MATERIALS AND METHODS

Animals

This study was performed on 15 domesticated dogs (Canis familiaris) of both sex (nine males and six females), they were collected from different localities all over Menoufia Governorate, Egypt. These animals were healthy without any diseases related to the eye or the head region. Additionally, the postmortem evaluation of the eye and adnexa were performed and the absence of any gross abnormalities. Handling of these animals and the research protocols according to guidelines of the University of Sadat City.

CT imaging

The selected heads were disarticulated at the atlanto-occipital joint then examined by CT imaging immediately within 30 minutes after collection. The study had performed in the rostrocaudal direction with the head kept in ventral position. Images had been obtained in the axial, coronal, sagittal planes using multidetector 128 – slice helical CT scanner (Fast, High-Speed CT scanner, Somatom Perspective, Mawda Radiology Centre, Shibine El- Kome, Egypt) of 130 kV, 180 mA, and slice thickness range from 0.6 to 1.5mm, scanning time rage from 8 to13 Sec., All images were being uploaded to DICOM viewer Radiant for data manipulation and measurements.

Data manipulation and measurements

In the soft-tissue window algorithm, a single examiner conducted manual contouring on each slice of the CT images.

Table (1): Intraocular parameters of dog eye:

Calculated data	Meaning
Eyeball and intraocular structures (Fig.1)	
a) Anteroposterior distance of the anterior chamber (ACHD)	Distance from the internal surface of the cornea to the anterior border of the lens.
b) Anteroposterior distance of the vitreous chamber (VCHD)	Distance from the posterior aspect of the lens to the internal surface of the choroid/retina/sclera.
c) Anterior-posterior distance of the lens (Axial length)	Taken at the widest dimension of the lens.
d) lateromedial distance of the lens (equatorial width)	Taken at the widest dimension of the lens.
e) Anteroposterior distance of the globe AGL (axial length)	From the internal surface of the cornea to the internal surface of the choroid/retina/sclera.
f) lateromedial distance of the globe (equatorial width)	Measured perpendicular to the axial length just caudal to the lens.
g) Radiodensity of vitreous and aqueous humor, and lens.	Multiplanar reconstruction (MPR) was used to obtain the radiodensities where the structures were visible to be measured, an area in the center of anterior chamber (≈4 mm^2), the vitreous chamber (≈10 mm^2), and the lens (≈ 20 mm^2) was performed.

Table (2): Orbital parameters of dog eye:

Orbit	
h) The horizontal orbital diameter (HOD) (Fig.2/ a)	Distance between medial wall to the point where a line drawn from the zygomatic process of the frontal bone intersects the zygomatic arch.
i) The vertical orbital diameter (VOD) (Fig.4/ d)	Between the inferior and superior orbital wall.
j) Orbital Area (OA)	22/7 ab, where a and b are half the orbital length and width, respectively.
k) Orbital Depth (OD)	Distance between the optic foramen and center of the orbital rim.
l) Globe position (Fig.4/ c)	Distance between the interzygomatic line and the posterior ocular surface was measured **(Gupta *et al.*, 2019)**.

The attenuation in Hounsfield Units (HU) of the vitreous humor, aqueous humor, and lens was measured. The procedure for taking measurements was followed exactly as defined in (Olopade et al., 2011) in the pig, (Salgüero et al., 2015) in canine, (Silva et al., 2017) in monkey, (Chandrakumar et al., 2019) in feline, (Lantyer-Araujo et al., 2019) in fox and dog. To maintain the independence of the variables, all comparisons between clinical data were made using the right and left eyes. All multiplanar planes in which globe size was optimized were used.

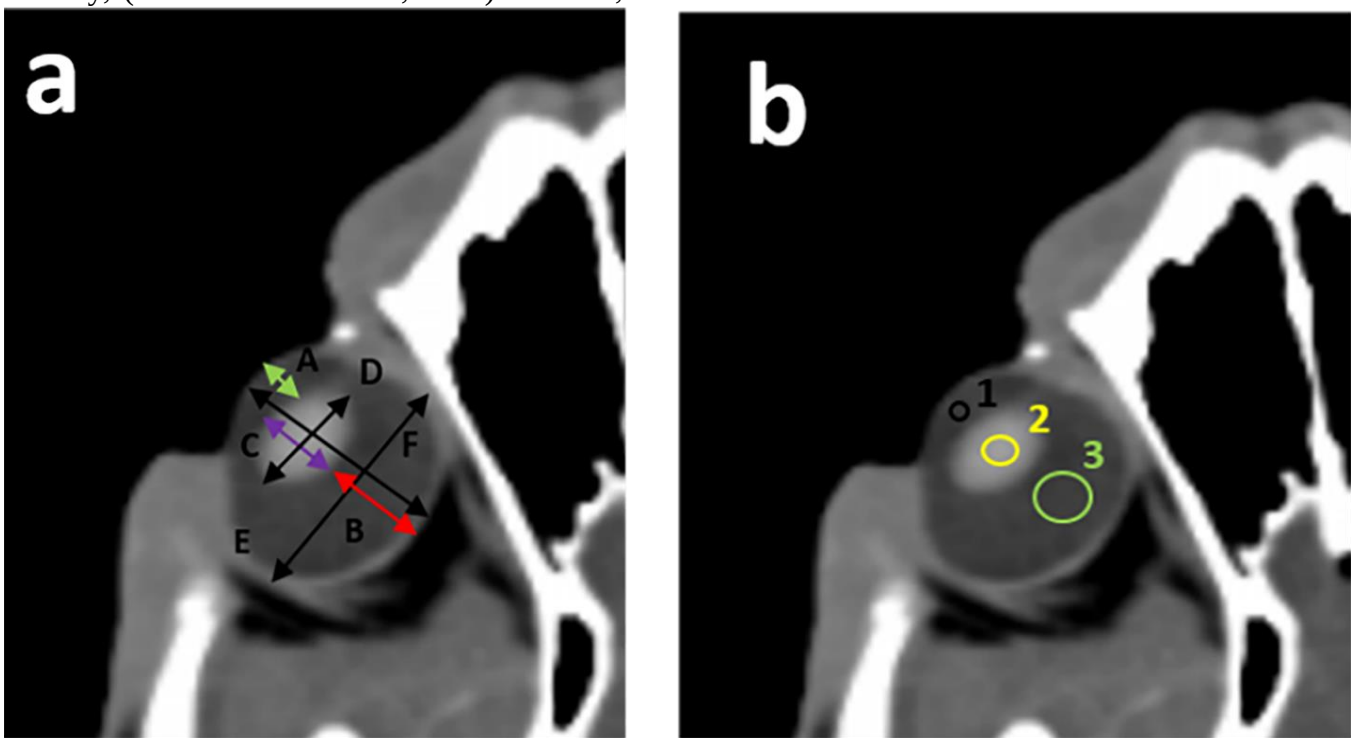

Figure (1): Soft tissue window of non-contrast CT scan, a- Axial plane of the globe detailing the measurements of **(A)** The anteroposterior distance of the anterior chamber, **(B)** The anteroposterior distance of the vitreous chamber, **(C)** The anteroposterior distance of the lens, **(D)** The lateromedial distance of the lens **(E)** The anteroposterior distance of the globe, and **(F)** The lateromedial distance of the globe. B- showing non-contrast CT scan Multiplanar reconstruction (MPR) in coronal plane of the

globe, where region of interest was placed in the middle of aqueous humour (1), lens (2), and vitreous humour (3) pointed to the density in Hounsfield (HU) of each structure.

Statistical Analysis

All the data obtained during the experiment were analyzed by IBM SPSS statistics (version 22) and expressed as Mean±SE. of total number of animals used in each group.

RESULTS

The spherical eye presented as a single layer tissue, CT images differentiated only the hyperattenuating lens, anterior chamber, vitreous chamber, and sclera–choroid–retina complex, however, the iris and ciliary body were not as clearly visualized (Fig. 4/a, b), the supraorbital process is replaced by an orbital ligament(Fig. 3/ a).Extraocularmuscle (Fig. 3). Medial rectus muscle appeared hypoattenuating tissue with ill definite contours, difficult to isolate it from other structures, and situated parallel to the frontal bone, but lateral rectus muscle situated parallel to the orbital ligament. Ventral oblique muscle appeared hypo attenuated, ventrally situated near the insertion of the ventral rectus muscle. Dorsal and ventral rectus appeared hypoattenuating tissue with ill definite contours and difficulty of following its caudal direction to optic foramen or isolate it from other structures.

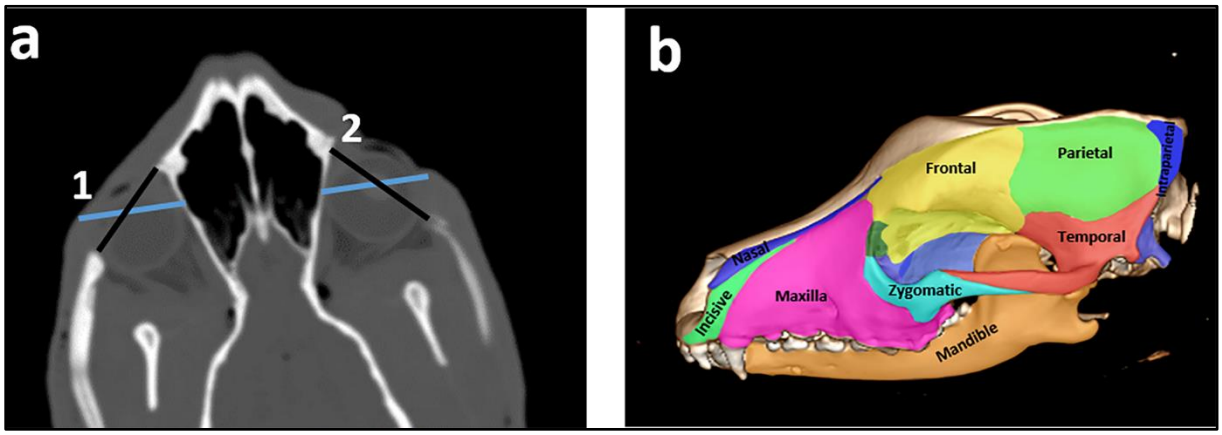

Figure (2): Non contrast CT and 3D reconstruction mages that illustrating, a- orbital diameters, b- orbital bones.

The lacrimal gland is situated ventrally to the orbital ligament, however periorbital fat between the ventral surface of the gland and the eyeball obstructed LG visualization, so difficult to determine its contour. Orbital cavity bounded by (Fig. 2/ b) frontal bone dorsally, ventrally by zygomatic bone, lacrimal bone rostral, caudally, supraorbital process replaced by an orbital ligament.

The parameter of the orbit was illustrated in (diagram 1.). The mean of right horizontal and vertical diameter were (2.71), (2.83) cm and left one were (2.72), (2.86) cm respectively, while on 3D was (2.58, 2.76) cm for right and (2.63, 2.77) cm for left one. Orbital index and orbital area of right were (104.00 %), (5.83 cm2), the left were (105.81%), (6.31 cm2). Whilst on 3D the right one were (103.71%), (5.51 cm2) and left were (107.37%), (5.85 cm2) respectively.

The right orbit had a mean of orbital depth (3.38 cm), but the left was (3.36 cm). The mean of the right opening angle of the orbit (68.50°) and (68.53°) of the left, the globe position mean was (0.59 cm), (0.61 cm) in right and left respectively.

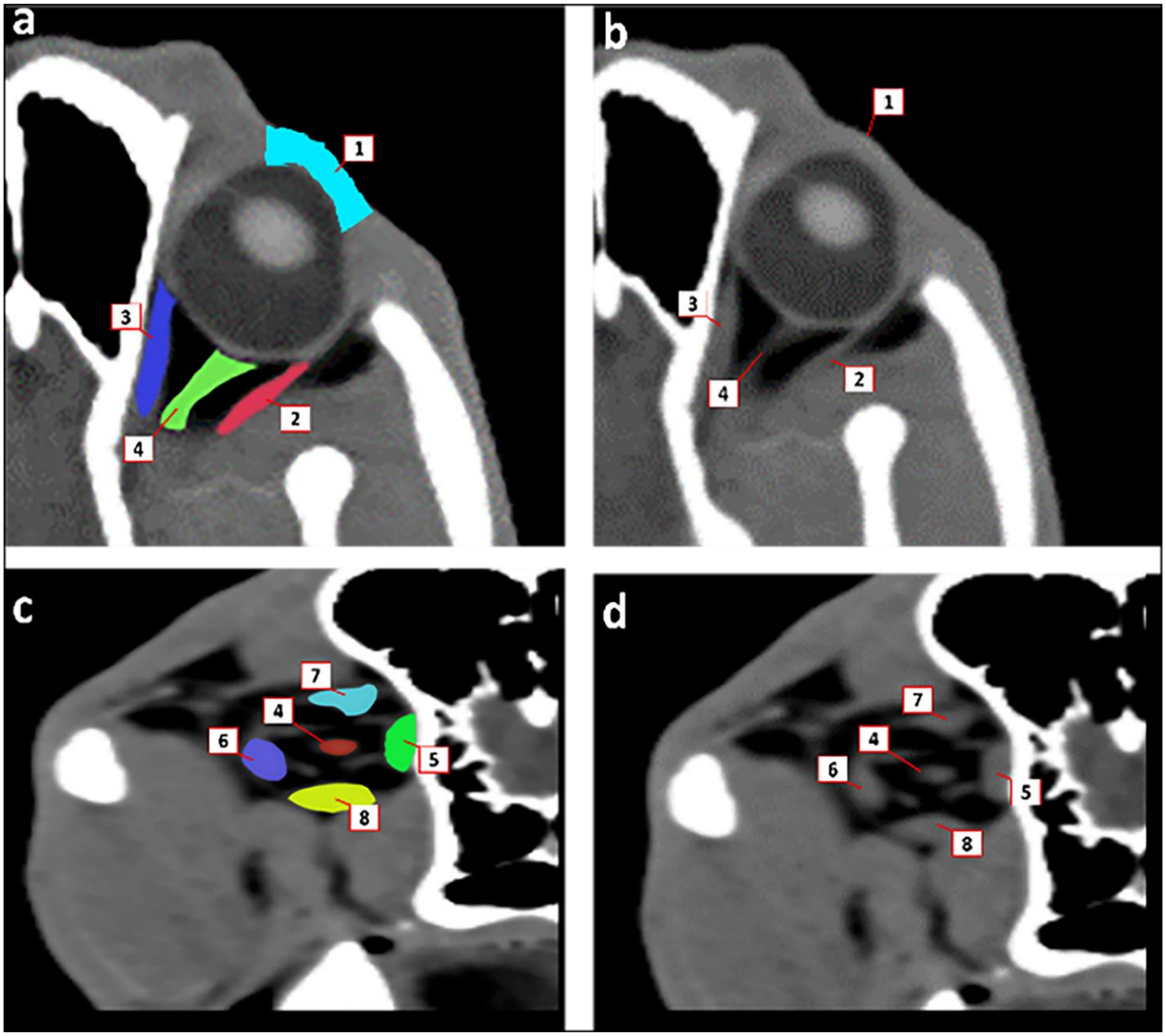

Figure (3): Non contrast CT image of eye and adnexa of dog axial plane of soft tissue showing, 1- orbital ligament, 2-ventral oblique muscle, 3- dorsal oblique muscle, 4- optic nerve, 5- medial rectus muscle, 6- lateral rectus muscle, 7- dorsal rectus muscle, 8- ventral rectus muscle, 8- optic nerve.

The measurements for the various intraocular structures of the left and right eye have been included (diagram 2.), the mean of right anterior chamber distance was (3.66 mm), while left eye means (3.28 mm).The density of the left aqueous humor which is hypodense and homogenous was (14.49 HU), whilst the right was (13.92 HU). The vitreous chamber filled with vitreous humor which is isodense to the aqueous humor, its density was (10.25 HU) in the right eye and (11.60 HU) in the left, its anteroposterior distance mean was (0.79, 0.76 cm) in right and left eye respectively. The dog's ocular right globe had a mean anteroposterior distance (1.98 cm), but the left one had a mean (1.96 cm). The mean of the left globe width was (1.79 cm), but the right was (1.75 cm).

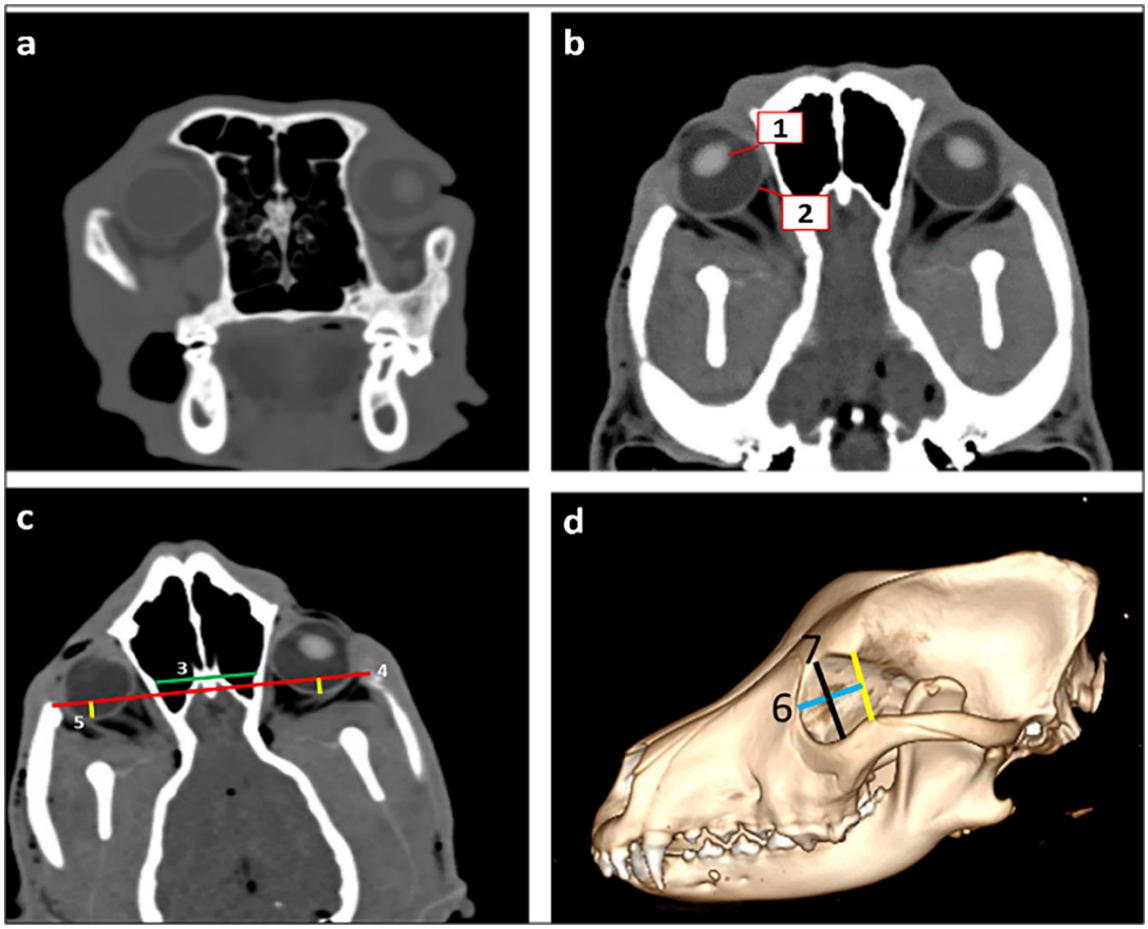

Figure (4): Non contrast CT and 3D reconstruction mages that illustrating, a- normal eye appearance in bone window axial plane, b & c- soft tissue bone showing, 1- lens, 2- choroid, sclera, and retina complex, 3- intra orbital distance, 4- intra zygomatic distance, 5- globe position.

The lens was hyperdense structure, had a mean anteroposterior length of (0.83, 0.83) cm in right and left eye respectively, its lateromedial distance was (1.02) cm in right and (1.00) cm in the left eye. The density mean in the center of the lens was (129.16) HU in right and (129.64) HU in the left.

Diagram (1): CT measurements of orbital parameters of dog:

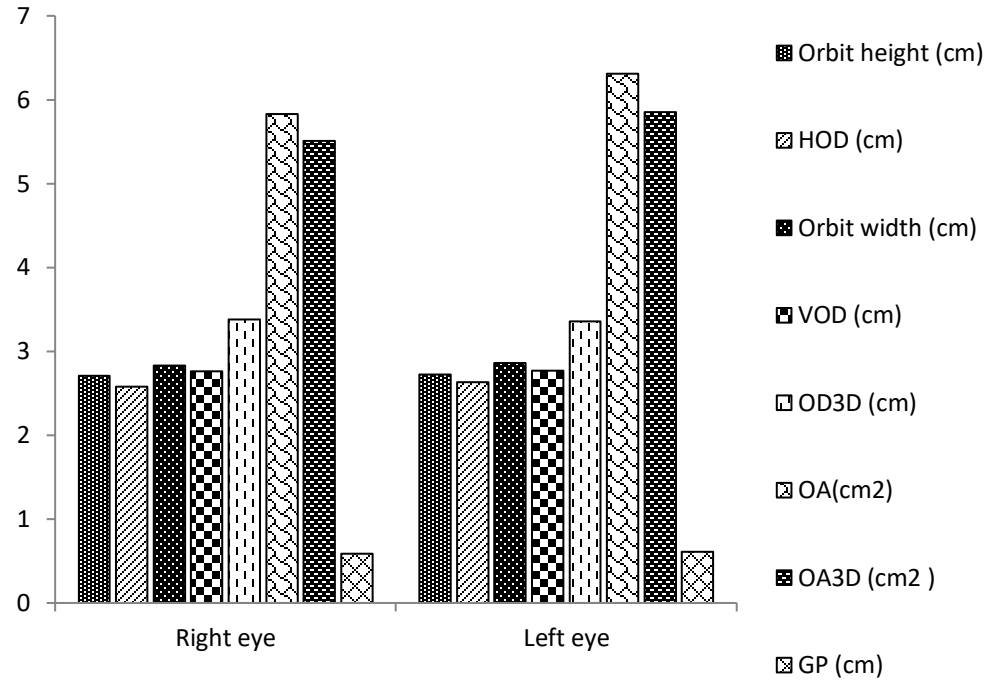

Diagram (2): CT measurements of intraocular parameters of dog.

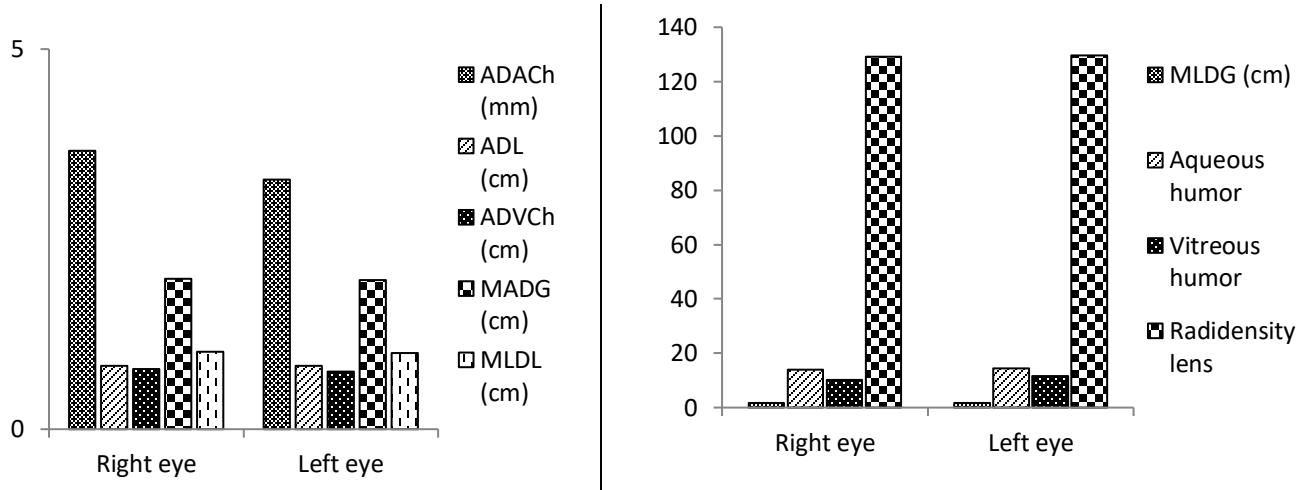

DISCUSSION

MRI and US are the diagnostic imaging modalities of choice for examination of eye and soft tissue. However, there is little literature concerning orbital CT in healthy dog.

Aqueous and vitreous humor were homogenous and hypodense, that agree with (Boroffka et al., 2006); (Kumawat & Jhirwal, 2021) in a dog, (McMullen & Gilger, 2006) in equine, (Kassab, 2012) in camel and buffalo, and (Al-Redah et al., 2016) in goat.

The hyperattenuating single layer appearance of the sclera–choroid–retina complex is similar to (Penninck et al., 2001); (Kumawat & Jhirwal, 2021) in the dog, (EL-Maghraby et al., 1995) in cattle and sheep, (Rogers et al., 1986) in the horse, and (Leszczyński et al., 2018) in pig by using Lugol staining procedures, however, disagree with (Leszczyński et al., 2018) when

used OsO4 staining procedures where the complex could be separated.

visualization of iris and the ciliary body does not affirm the finding of (Potter et al., 2008),(Ribeiro et al., 2009), (Kassab, 2012) as appeared hyperechoic, and the finding of (Scotty et al., 2004),(Kumawat &Jhirwal, 2021) where they appeared at the lateral margins of the lens, but their appearance was agreed with (Leszczyński et al., 2018) when used OsO4 staining procedures.

With regards to the lens, it has to be noted that the hyperattenuating lens disagrees with (Potter et al., 2008),(Ribeiro et al., 2009), (Kassab, 2012),(Leszczyński et al., 2018), (Kumawat & Jhirwal, 2021), who described it as anechoic and appeared as two curvilinear echogenicities representing lens capsules. However agree with (Madkour et al., 2016) in goats, (Salgüero et al, 2015),(Chandrakumar et al., 2019) in canine and feline respectively.

Regarding radiodensity, the values that have been found may be useful for radiation therapy purposes. It's critical to avoid doses to organs at risk, such as the lens. The accurate calculation of the expected doses each of these structures will receive while planning radiation therapy for nasal tumors will be allowed by inputting appropriate HU for each of these structures.

The density of lens, anterior and vitreous chamber were similar to (Salgüero et al**.,** 2015) without contrast, but different from (Chandrakumar et al., 2019), where the density of anterior and vitreous chamber of our result higher than that of feline either pre or post-contrast, in contrast, the density of feline lens was higher than our finding, this may be attributed due to difference across species and age.

The intraocular parameters, for instance, axial globe length and Equatorial width were similar to (Mirshahi et al., 2014), (Vinas et al., 2019), smaller than (Salgüero et al., 2015), (Chandrakumar et al., 2019), (Kovaļčuka & Mūrniece, 2020),(Yilmaz & Durmaz, 2021), however higher than (Gonçalves et al., 2000) due to variance in breed size and body weight.

The axial length of the lens was similar to (Salgüero et al., 2015), (Chandrakumar et al**.**, 2019) higher than (Mirshahi et al**.**, 2014), (Vinas et al**.**, 2019), (Kovaļčuka & Mūrniece, 2020), however smaller than (Vosough et al., 2009), (Yilmaz & Durmaz, 2021**)**. Thoroughly indicated this due to differences in species, breed, age, and body weight (Mirshahi et al., 2014).

Vitreous chamber depth was similar to **(**Chandrakumar et al., 2019), (Yilmaz & Durmaz, 2021)**,** but smaller than **(**Mirshahi et al., 2014), (Salgüero et al., 2015), (Vinas et al., 2019**)** this may be due to breed difference. Anterior chamber depth was higher than (Cottrill et al**.**, 1989**)** due to the use of the recoil pad, which avoids the condensation of the cornea and anterior and posterior chamber, however similar to **(**Salgüero et al., 2015), (Chandrakumar et al., 2019**)**. Orbital parameters were similar to **(**Lantyer-Araujo et al., 2019**)** except for orbital depth which is smaller, this may be attributed due to the view from which we have calculated depth or due to the change in breed and body weight.

CONCLUSION

Computed tomography is a valuable diagnostic technique for the examination of the eye, and this study provided a valuable reference for the dimension of the intraocular parameters where these measurements can be used as a basis for further clinical diagnosis of ocular abnormalities.

ACKNOWLEDGEMENTS

This research was partially supported by the Faculty of veterinary medicine, University of Sadat City. This study is summarized from the master thesis.

CONFLICTS OF INTEREST

The authors do not have any conflicts of interest to declare.

REFERENCES

Al-Redah, S.A.A., Al-Hacham, E.E.D., Al-Sharoot, H.A. (2016).). ULTRASONOGRAPHIY OF THE EYE IN SHEEP. Basrah Journal of Veterinary Research, 15(2).

Boroffka, S. A., Görig, C., Auriemma, E., PASSON-VASTENBURG, M. H., Voorhout, G., & Barthez, P. Y. (2008). Magnetic resonance imaging of the canine optic nerve. Veterinary Radiology & Ultrasound, 49(6), 540-544.

Boroffka, S. A., Voorhout, G., Verbruggen, A. M., & Teske, E. (2006). Intraobserver and interobserver repeatability of ocular biometric measurements obtained by means of B-mode ultrasonography in dogs. American journal of veterinary research, 67(10), 1743-1749.

Chandrakumar, S. S., Zur Linden, A., Owen, M., Pemberton, S., Pinard, C. L., Matsuyama, A., & Poirier, V. J. (2019). Computed tomography measurements of intraocular structures of the feline eye. Veterinary Record, 184(21), 651-651.

Chiwitt, C. L., Baines, S. J., Mahoney, P., Tanner, A., Heinrich, C. L., Rhodes, M., & Featherstone, H. J. (2017). Ocular biometry by computed tomography in different dog breeds. Veterinary ophthalmology, 20(5), 411-419.

Cottrill N.B, Banks W.J, Pechman R.D. Ultrasonographic and biometric evaluation of the eye and orbit of dogs. Am. J. Vet. Res. 1989;50(6):898–903.

Dennis, R. (2000). Use of magnetic resonance imaging for the investigation of orbital disease in small animals. Journal of Small Animal Practice, 41(4), 145-155.

El-Maghraby, H. M., Nyland, T. G., & Bellhorn, R. W. (1995). Ultrasonographic and biometric evaluation of sheep and cattle eyes. Veterinary Radiology & Ultrasound, 36(2), 148-151.

El-naseery, N. I., El-behery, E. I., El-Ghazali, H. M., & El-Hady, E. (2016). The structural characterization of the lacrimal gland in the adult dog (Canis familiaris). Benha Veterinary Medical Journal, 31(2), 106-116.

Gonçalves, G., F., Pippi, N.L., Raiser, A.G., Mazzanti, A., Oliveira, S.T., Neves, J.P., Leotte, A.M. and Hintz, C.W. (2000) Two-dimensional real-time ultrasonic biometry of ocular globe of dogs. Cienc. Rural, 30(3): 417-420.

Gupta, V., Prabhakar, A., Yadav, M., & Khandelwal, N. (2019). Computed tomography imaging-based normative orbital measurement in Indian population. Indian journal of ophthalmology, 67(5), 659.

Kassab, A. (2012). Ultrasonographic and macroscopic anatomy of the enucleated eyes of the buffalo (Bos bubalis) and the one-humped camel (Camelus dromedarius) of different ages. Anatomia, histologia, embryologia, 41(1), 7-11.

Kovaļčuka, L., & Mūrniece, G. (2020). Normal reference ranges of ocular physiology and sonographic biometry of Latvian Hunting dogs. Veterinary world, 13(4), 807.

Kumawat, N. K., & Jhirwal, S. K. (2021). B-mode ultrasonographic appearance of the globe and intraocular structures of eye in dogs. The Pharma Innovation Journal SP-10 (2), 68-71.

Lantyer-Araujo, N. L., Silva, D. N., Estrela-Lima, A., Muramoto, C., De Azevedo Liborio, F., Da Silva, E. A., & Oria, A. P. (2019). Anatomical, histological and computed tomography comparisons of the eye and adnexa of crab-eating fox (Cerdocyon thous) to domestic dogs. PLoS ONE, 14(10), e0224245.

Leszczyński, B., Sojka-Leszczyńska, P., Wojtysiak, D., Wróbel, A., & Pędrys, R. (2018). Visualization of porcine eye anatomy by X-ray microtomography. Experimental eye research, 167, 51-55.

Madkour, N., Amin, M., Karkoura, A. A., Alsafy, M. A., & El-Gendy, S. A. (2016). Computed Tomography and Gross Anatomical Studies of the Orbital Cavity of the Baladi Goat (Capra hircus). Alexandria Journal for Veterinary Sciences, 51(2).

McMullen Jr, R. J., & Gilger, B. C. (2006). Keratometry, biometry and prediction of

intraocular lens power in the equine eye. Veterinary Ophthalmology, 9(5), 357-360.

Mirshahi, A., Shafigh, S. H., & Azizzadeh, M. (2014). Ultrasonographic biometry of the normal eye of the Persian cat. Australian veterinary journal, 92(7), 246-249.

Morgan, R. V., Daniel, G. B., & Donnell, R. L. (1994). Magnetic resonance imaging of the normal eye and orbit of the dog and cat. Veterinary Radiology & Ultrasound, 35(2), 102-108.

Olopade, J. O., Igado, O. O., Azeez, I. A., & Okandeji, M. E. (2011). Morphometric studies of the eyeball and orbital region of the Nigerian local pig (Sus scrofa). Tropical Veterinarian, 29(1), 34-40.

Penninck, D., Daniel, G. B., Brawer, R., & Tidwell, A. S. (2001). Cross-sectional imaging techniques in veterinary ophthalmology. Clinical techniques in small animal practice, 16(1), 22-39.

Potter, T. J., Hallowell, G. D., & Bowen, I. M. (2008). Ultrasonographic anatomy of the bovine eye. In Veterinary Radiology and Ultrasound (Vol. 49, Issue 2, pp. 172–175).

Ribeiro, A. P., Silva, M. L., Rosa, J. P., Souza, S. F., Teixeira, I. A., & Laus, J. L. (2009). Ultrasonographic and echobiometric findings in the eyes of Saanen goats of different ages. Veterinary ophthalmology, 12(5), 313-317.

Rogers, M., Cartee, R. E., Miller, W., & Ibrahim, A. K. (1986). Evaluation of the extirpated equine eye using B-mode ultrasonography. Veterinary Radiology, 27(1), 24-29.

Salgüero, R., Johnson, V., Williams, D., Hartley, C., Holmes, M., Dennis, R., & Herrtage, M. (2015). CT dimensions, volumes and densities of normal canine eyes. Veterinary Record, 176(15), 386-386.

Scotty, N. C., Cutler, T. J., Brooks, D. E., & Ferrell, E. (2004). Diagnostic ultrasonography of equine lens and posterior segment abnormalities. Veterinary ophthalmology, 7(2), 127-139.

Singh, S., Purohit, S., & Pandey, R. P. (2015). B-MODE INTRAOCULAR ECHO-MORPHOMETRY OF MURRAH BUFFALO (Bubalus bubalis). Ruminant science, 249.

Vinas, M., Zeyen, U. L. R. I. C. H., D'Anna, N. U. N. Z. I. O., & Vignoli, M. (2019). Transscleral ultrasonographic measurements of the optic nerve sheath diameter and a regression analysis with morphometric measures of the globe in dogs. Veterinární medicína, 64(11), 490-496.

Vosough, D., Shojaei, B., & Molazem, M. (2009). Magnetic resonance imaging of feline eye. Iranian Journal of Veterinary Research, 10(1), 66-69.

Yilmaz, O., & Durmaz, F. (2021). Examining the morphometric features of bulbus oculi in Van cats by using computed tomography and magnetic resonance imaging. Ankara Üniversitesi Veteriner Fakültesi Dergisi.